Re-examination of the Observed Decadal Variability of Earth Radiation Budget using Altitude-corrected ERBE/ERBS Nonscanner WFOV Data

Takmeng Wong*, Bruce A. Wielicki, and Robert B. Lee, III

NASA Langley Research Center, Hampton, VA

G. Louis Smith

National Institute of Aerospace, Hampton, VA

Kathryn A. Bush

Science Applications International Corporation, Hampton, VA

Josh K. Willis

California Institute of Technology, Pasadena, CA

Revised for the Journal of Climate

November 2005

*Corresponding author address: MS 420, NASA Langley Research Center, Hampton, VA, 23681-2199; email: takmeng.wong@nasa.gov

Abstract

This paper gives an update on the observed decadal variability of Earth Radiation Budget using the latest altitude-corrected Earth Radiation Budget Experiment (ERBE)/Earth Radiation Budget Satellite (ERBS) Nonscanner Wide Field of View (WFOV) instrument Edition3 dataset. The effects of the altitude correction are to modify the original reported decadal changes in tropical mean (20N to 20S) longwave (LW), shortwave (SW), and net radiation between the 1980s and the 1990s from 3.1/-2.4/-0.7 to 1.6/-3.0/1.4 Wm^{-2} respectively. In addition, a small SW instrument drift over the 15-year period was discovered during the validation of the WFOV Edition3 dataset. A correction was developed and applied to the Edition3 dataset at the data user level to produce the WFOV Edition3_Rev1 dataset. With this final correction, the ERBS Nonscanner observed decadal changes in tropical mean LW, SW, and net radiation between the 1980s and the 1990s now stand at 0.7/-2.1/1.4 Wm^{-2}, respectively, which are similar to the observed decadal changes in the HIRS Pathfinder OLR and the ISCCP FD record; but disagree with the AVHRR Pathfinder ERB record. Furthermore, the observed inter-annual variability of near-global ERBS WFOV Edition3_Rev1 net radiation is found to be remarkably consistent with the latest ocean heat storage record for the overlapping time period of 1993 to 1999. Both data sets show variations of roughly 1.5 Wm^{-2} in planetary net heat balance during the 1990s.

1. Introduction

Continuous monitoring of the Earth radiation budget (ERB) at the top of atmosphere (TOA) is essential for understanding climate and climate variability on Earth. Wielicki et al. (2002a) reported large decadal changes in tropical mean (20N to 20S) Earth radiation budget between the 1980s and the 1990s based on the longest running single ERB time series produced from the Earth Radiation Budget Experiment (ERBE; Barkstrom, 1984) Earth Radiation Budget Satellite (ERBS) Nonscanner Wide Field of View (WFOV) instrument Edition2 data record. The results also were based on a range of overlapping scanning and nonscanning ERB instruments; including Nimbus-7 Nonscanner (Bess et al., 1989), ERBE/ERBS Scanner, the Scanner for Radiation Budget (ScaRaB) instrument (Kandel et al., 1998) on the Meteor satellite, the ScaRaB Scanner (Duvel et al., 2001) on the Resurs Satellite, the Clouds and the Earth's Radiant Energy System (CERES, Wielicki et al., 1996) Scanner on the TRMM satellite and the CERES Scanner on the Terra Satellite.

Since that report, a complete re-examination of the ERBE/ERBS Nonscanner WFOV dataset, prompted by new findings on the possible effect of small but significant ERBS altitude changes over the 15-year period, has been completed. This satellite altitude change and its effects on the top of the atmosphere ERB are discussed in section 2 using the new altitude-corrected WFOV Edition3 dataset. Section 3 presents results on a small WFOV shortwave instrument drift and its effects on the ERB record. This instrument drift was discovered during the validation of the WFOV Edition3 dataset and is not currently included in the archived WFOV Edition3 data, but a simple correction method is available to the data user to remove this instrument artifact. Sections 4 and 5

compare the latest ERBS Nonscanner WFOV record with existing satellite-based time series of ERB from the High Resolution Infrared Radiation Sounder (HIRS) Pathfinder Outgoing longwave radiation (OLR, Mehta and Susskind, 1999) dataset, the International Satellite Cloud Climatology Project (ISCCP) FD dataset (Zhang et al., 2004), and the Advanced Very High Resolution Radiometer (AVHRR) Pathfinder ERB dataset (Stowe et. al., 2002), as well as records from the most recent ocean heat storage dataset based on both ocean in-situ vertical soundings and satellite altimeter measurements (Willis et al. 2004). Summary and conclusions are given in Section 6. Additional information concerning the ERBS Nonscanner data processing and the error estimates for the TOA radiation datasets used in this study are provided in Appendices A and B.

2. Altitude-corrected WFOV Edition3 data

ERBS altitude (shown in Figure 1) slowly dropped from 611 km to 585 km over the first 15 years of the mission. The satellite altitude is defined as height above sea level. The changes in satellite altitude can directly affect the ERBS Nonscanner WFOV TOA fluxes through the ERBS Nonscanner inversion process in which satellite altitude observed fluxes are converted to TOA fluxes (Lee et al., 2003). Unlike the ERBE scanner instrument, which sees only small portions of the Earth surface with a 40-km nadir field of view, the Nonscanner WFOV instrument field-of-view at satellite altitude contains the entire earth disk and a small ring of surrounding deep space. The amount of energy received at the Nonscanner WFOV instrument is therefore inversely proportional to the square of the distance between the instrument and the Earth's center. As the altitude dropped over the 15-year period, the Nonscanner WFOV instrument recorded a small

steady increase in satellite altitude fluxes. The ERBS WFOV Edition2 data analysis system was designed to account for changes in satellite altitude, but the original algorithm designed this function to provide a correction in the case of a non-circular satellite orbit. It was recently discovered that the altitude correction was disabled in the case of a near-circular orbit, and therefore did not apply to correct the average spacecraft altitude change that occurred later in the extended ERBS mission. The main effect of this altitude change is a small increase (~0.6 %) in both TOA outgoing longwave radiation (LW) and reflected shortwave radiation (SW) over the 15-year period.

Based on this new information, the entire ERBE/ERBS Nonscanner WFOV Edition2 data record was reprocessed to Edition3 data using a set of time dependent correction coefficients derived from time series of the ERBS altitude record. Figure 2 shows the time series of 36-day averaged tropical mean (20N to 20S) ERBS Nonscanner WFOV radiative energy budget with (Edition3, solid lines) and without (Edition2, dotted lines) this satellite altitude correction. The 36-day mean is used to reduce diurnal aliasing in the Nonscanner dataset resulting from a shift in the local time of satellite observations over the 15-year period (Wielicki et al., 2002b). Figure 2 is in the form of deseasonalized anomalies with respect to the 1985 to 1989 climatology. This was done because the seasonal cycles in LW, SW, and net flux are large enough to make decadal variability difficult to visualize. The effect of the altitude correction is to reduce the magnitude of the tropical LW flux change from the 1980s to 1990s from the original 3.1 to 1.6 Wm^{-2}. The correction increases the magnitude of the SW flux decadal change from –2.4 to –3.0 Wm^{-2}. The correction also changes the sign and the magnitude of the net radiation

decadal change from –0.7 Wm^{-2} (cooling of the tropics) to 1.4 Wm^{-2} (heating of the tropics).

3. WFOV Shortwave Instrument Drift

In addition to the satellite altitude decrease over the 15-year period, the ERBS WFOV shortwave instrument also appears to have a residual instrument trend that is not fully corrected by using the bi-weekly solar constant calibrations. This shortwave instrument trend, on the level of 1% over the 15-year period, was discovered during the validation of the ERBE/ERBS WFOV Edition3 dataset. The mostly likely cause of this shortwave trend, based on the most recent instrument engineering study (Smith et al. 2002), is due to non-uniform exposure of the Nonscanner WFOV shortwave sensor dome to UV radiation during spacecraft sunrise and sunset over the 15-year period. In particular, the sides of the SW filter dome on the Nonscanner WFOV instrument receive more UV exposure than the top of the dome. This can lead to a slight difference in the dome transmission between viewing a small angle of view source like the sun, versus a wide angle of view target like the Earth. Since the Nonscanner WFOV instrument does not carry a dedicated longwave sensor, the longwave fluxes during daytime are determined from the total channel (0.2 to 100 micron) minus the shortwave channel (0.2 to 5 micron). Thus, this residual shortwave instrument trend can also directly affect the reported daytime longwave fluxes. During nighttime, the longwave fluxes are determined directly from the total channel since there are no solar reflected shortwave signals at night.

Figure 3 shows the time series of daytime longwave flux (red curve), nighttime longwave flux (blue curve) and day-minus-night longwave flux difference (green curve) over the tropics from the ERBS Nonscanner WFOV Edition3 data record over the 15-year period. These time series are deduced directly from instantaneous grid box data and contain slightly more sampling noise than the traditional monthly mean data. The periodic features in both the daytime longwave and nighttime longwave time series are caused by the semi-annual cycle of longwave radiation in the tropics as the Sun marches in and out of the tropical belt every six months. Nevertheless, the figure clearly shows that the day-minus-night longwave difference is slightly increasing over time. This results from the fact that the nighttime longwave shows little change, but the daytime longwave has increased significantly over the same period. Figure 3 suggests that the WFOV total channel is stable over time (consistent with solar constant checks), but the WFOV shortwave channel has drifted slightly over the same period. Basically, the shortwave dome has degraded slightly over time and allows less solar energy onto the WFOV shortwave detector, thus artificially producing a lower shortwave flux and a higher longwave flux during daytime. Note that the WFOV total channel has no dome over the cavity, so that this transmission loss is not applicable to the total channel.

The ERBS Nonscanner measurements discussed up to this point are based on data from the Wide Field of View (WFOV) instruments. The ERBS Nonscanner instrument package also contains a set of Medium Field of View (MFOV) instruments that record the Earth reflected solar and total spectrum energy with an effective field of view of about 800 km diameter. These MFOV instruments are adjacent to the WFOV instruments on the ERBS spacecraft. Unlike the WFOV instruments, the MFOV sensors are

completely shielded from the Sun during Earth viewing operation. Therefore the MFOV data should show no trend in the day minus night longwave flux over this period. This is evident in Figure 4, which shows the MFOV daytime longwave flux, nighttime longwave flux and day minus night longwave flux difference time series over the ERBS 15-year period. The day minus night MFOV longwave flux differences, the daytime longwave flux, and nighttime longwave flux are very stable over this time period. The short time scale noise of these fluxes, however, is much larger than the WFOV, since the MFOV covers the daytime tropics only once every 4 days. This can be simply understood as the spatial scale of the ~800km diameter MFOV observation centered on the satellite ground-track, ratioed to the typical distance between satellite orbit tracks of ~2700km. The effective diameter of the WFOV measurement is ~ 1500km (Green and Smith, 1991). There is also a second limitation of the MFOV data. Unlike the WFOV, a complete range of nadir to limb viewing zenith angles of earth radiation are not viewed, and therefore much larger scene dependent corrections of the MFOV measurement are required to estimate TOA flux (Green and Smith, 1991). As a result of these issues, the MFOV data was never the primary ERBS Nonscanner TOA flux data set, but remained an off-line quality control data set. The longer the time period of interest, however, the more useful the MFOV data becomes.

The MFOV data, while noisy, supports the hypothesis that non-uniform solar exposure on the Nonscanner WFOV SW dome has caused the observed drift in the Nonscanner WFOV measurement over the 15-year period. The differences in the absolute value between the WFOV longwave (Figure 3) and MFOV longwave (Figure 4) are caused by differences in absolute calibration, inversion algorithm (anisotropy

correction), spatial sampling, and the much larger effect of the field of view limiter on the MFOV cavity. These differences are representative of the absolute accuracy uncertainty between these two datasets. The long-term stability performance of these two instrument packages, which is most important for long-term climate change study, has been deduced from observations and is found to be remarkably similar to each other with both showing high stability over ERBS mission lifetime (See Appendix B for WFOV stability uncertainty).

A correction for this shortwave sensor trend is derived from the WFOV Edition3 dataset using a simple linear trend removal of the drift shown in Figure 3. The correction is applied to the WFOV Edition3 time series shown in Figure 2. This shortwave sensor drift corrected data will now be referred to as WFOV Edition3_Rev1 data. Note that the WFOV SW sensor trend correction is not currently included in the archived WFOV Edition3 dataset. However, this correction is available to data users through the online ERBE/ERBS S10N WFOV Edition3 data quality summary at the NASA Langley Atmospheric Science Data Center (http://eosweb.larc.nasa.gov/PRODOCS/erbe/quality_summaries/s10n_wfov/erbe_s10n_wfov_nf_sf_erbs_edition3.html) so they can apply the correction directly to the WFOV Edition3 data in future studies.

In general, the shortwave sensor drift correction further reduces the magnitude of the tropical mean decadal changes in LW flux from 1.6 Wm^{-2} to about 0.7 Wm^{-2}, and reduces the magnitude of the tropical mean decadal changes in SW flux from -3.0 Wm^{-2} to about -2.1 Wm^{-2} between the 1980s and the 1990s. Note that the change in WFOV SW channel has no effect on net flux trends, which remain at 1.4 Wm^{-2}. Net fluxes depend only on the WFOV total channel, which has no dome degradation, and has shown

consistency in solar calibration to 0.1% over the first 15 years of the ERBS mission (Lee et al., 2002).

Figure 5 shows an updated comparison of the new ERBS Nonscanner WFOV Edition3_Rev1 deseasonalized tropical mean (20N to 20S) flux anomalies time series to the same climate model simulations used in Wielicki et al. (2002a). The climate models include the Hadley Centre atmospheric climate model HadAM3 (Pope et al., 2000 and Sexton et al., 2001), the National Center for Atmospheric Research (NCAR) model CCM3 (Kiehl et al., 1998), the Geophysical Fluid Dynamics Laboratory (GFDL) climate model (Lau and Nath, 2001), and the GFDL EP (Experimental Prediction) model (Gordon et al., 2000). We also included the National Center for Environmental Prediction (NCEP)-NCAR 50-year Reanalysis, which uses NCEP 4-D assimilation model (Kistler et al., 2001). For all model runs, the deseasonalized tropical mean flux anomalies were calculated as in the satellite data, using the 1985 through 1989 period as the baseline. The comparison between Nonscanner WFOV Edition3_Rev1 deseasonalized LW anomalies and climate models is now in much better agreement, with the exception of the 1998 El Nino anomaly peak, but sizeable differences in deseasonalized SW flux and net flux anomalies remain. Note that the 1991 to 1993 Mt. Pinatubo aerosol signal was not provided to the climate models for the simulations, and they should not be expected to show these anomalies.

4. Comparison with other satellite-based decadal Earth radiation budget records

Several satellite-based decadal Earth radiation budget datasets of varying quality are available to the public. This section compares many of the currently available data

sets. Figure 6 shows a comparison of the ERBE/ERBS Nonscanner WFOV Edition3_Rev1 deseasonalized tropical mean (20N to 20S) radiative anomaly record against deseasonalized anomalies from HIRS Pathfinder OLR data, AVHRR Pathfinder ERB data, and ISCCP FD data. All anomalies are determined consistently using the base climatological period as 1985-1989 as in Wielicki et al. (2002a). For the LW component of the ERB, the four different datasets are consistent with each other during the first half of the data record. During the second half of the data record, the ERBS Nonscanner LW, HIRS Pathfinder OLR, and the ISCCP FD LW are in close agreement. The AVHRR Pathfinder LW, however, shows much lower values than the other time series during the later part of this data record. These problems are the result of instrument intercalibration and satellite orbit changes (time of day sampling) as discussed in Jacobowitz et al. (2003).

For the SW component of the ERB, the ERBS Nonscanner WFOV Edition3_Rev1 and the ISCCP FD data again agree well with each other over the entire span of the data period. HIRS Pathfinder provides only LW fluxes, so no SW or net flux comparisons are possible. The AVHRR Pathfinder SW data do not agree well with the two other datasets. The AVHRR data contain large shifts throughout the time series, again consistent with issues of intercalibration and changes in satellite orbit diurnal sampling.

The net component of the ERB is the combined effect of both LW and SW fluxes. While both the ERBS Nonscanner WFOV Edition3_Rev1 data and the ISCCP FD data are very similar to each other, the AVHRR Pathfinder net data again diverge from the other two datasets. Table 1 further summarizes the results of decadal changes in Earth radiation budget between the 1980s and the 1990s for these four datasets and the ERBS

Nonscanner WFOV Edition2 and Edition3 datasets. In general, there is good agreement among ERBS Nonscanner WFOV Edition3_Rev1, HIRS Pathfinder OLR and ISCCP FD data record. All three datasets show similar decadal changes in ERB with the same sign and similar magnitude. The AVHRR Pathfinder ERB dataset, however, disagrees with the other three datasets in both sign and magnitude. Jacobowitz et al. (2003) showed a promising technique for reducing these data problems in the current AVHRR Pathfinder ERB dataset. This corrected AVHRR Pathfinder dataset, however, is still under development and is not yet available to the public. An examination of Figure 4 from Jacobowitz et al. (2003) indicates that the comparable numbers for Table 1 would be about –2 Wm^{-2} for LW flux, +2 Wm^{-2} for SW flux, and near 0 for net flux. But inter-satellite shifts of 4 to 5 Wm^{-2} occur even in the corrected AVHRR Pathfinder data from Jacobowitz et al. (2003). We conclude that both the AVHRR pathfinder and the corrected AVHRR Pathfinder ERB datasets are not sufficiently accurate to resolve decadal changes in tropical mean or global scale radiative fluxes. They may be more useful for regional climate signals, but these are not compared here. A discussion of the accuracy of these data sets is given in Appendix B.

5. Comparison with ocean heat storage data

Willis et al. (2004) provides new estimates of annual global ocean heat storage for 1992 to 2002 using a combination of improved in-situ temperature profile sampling and constraints on thermal expansion from satellite global ocean altimeter observations. The major advantage of this dataset over previous ocean estimates is the use of global altimeter data to supplement sparse in-situ sampling in the southern hemisphere oceans.

On a global annual scale, the change in TOA net radiation and ocean heat storage should be in phase and of the same magnitude. This is due to the fact that all other forms of heat storage in the Earth system are factors of 10 or more smaller than ocean heat storage (Levitus, 2001). Previous ocean heat storage data sets required 5 to 10 year averages to reduce sampling errors. The Willis et al. (2004) analysis demonstrated a sampling error of 0.4 Wm^{-2} (1σ) for global annual ocean heat storage.

Figure 7 gives a direct interannual comparison of these new ocean heat storage data from 1993 to 2003 against those from the 12-month running mean ERBE/ERBS Nonscanner WFOV Edition3_Rev1 and CERES/Terra Scanner ES4 Edition2_Rev1 net flux anomalies. The CERES/Terra Scanner results are global and the ERBE/ERBS Nonscanner WFOV results cover 60N to 60S (or ~87% of the Earth surface). The net flux anomalies are calculated with respect to the 1985 to 1989 period. They are basically deseasonalized anomalies similar to those shown in previous figures. A 12-month running mean filter has been applied to the TOA radiation data to reduce the temporal sampling noise and to match-up directly with the corresponding time scale of the ocean storage data. The ocean heat storage data (Willis et al., 2004) is available only in annually smoothed seasonal data. The drop in the global ocean heat storage in later part of 1998 is associated with cooling of the global ocean after the rapid warming of the ocean during the 1997-1998 El Nino event (Willis et al., 2004). While spatial sampling error is the dominant source of uncertainty in the ocean data, absolute calibration uncertainties dominate the radiation budget data. For a comparison of interannual variations, however, we can remove the mean calibration uncertainty by requiring agreement for the average of all overlapping data for each instrument time series (e.g.

1993 to 1999 average for ERBS and ocean heat storage). Note that Willis et al. (2004) estimate the 10 year average uncertainty in ocean heat storage from 1992 to 2002 as ~ 0.2 Wm^{-2}. The interannual variability of the net flux anomalies in Figure 7 from the ERBS Nonscanner WFOV and CERES Scanner agree very well with the interannual variability of the ocean heat storage data. The agreement is within the ocean heat storage sampling uncertainties, with 1-sigma difference in the anomalies of 0.4 Wm^{-2}. The two times series are in phase with each other, consistent with the constraint of planetary energy balance.

This is a remarkable result given the totally independent physical measurement and sampling of the ocean heat storage data and the ERB datasets. The net flux anomalies within a single decade can be as large as 1.5 Wm^{-2} according to both the ERB and the ocean storage data. The data agree that the ERBS Nonscanner WFOV net radiation anomalies shown in Figure 5 are accurate to better than 0.5 Wm^{-2}, which is consistent with the estimated uncertainty of the ERBS WFOV data given in Appendix B. The large 1.5 Wm^{-2} change is most likely dominated by changes in cloudiness since aerosol radiative forcing estimates for this period show no large changes beyond the 1991-1993 Mt. Pinatubo cooling.

6. Summary and Conclusions

The original and Edition2 ERBE/ERBS Nonscanner WFOV data contain small systematic errors that can affect the interpretation of decadal changes. Specifically, ERBS altitude slowly dropped from 611 km to 585 km over the 15-year period. This introduces a 0.6% correction to the decadal changes reported in a previous study. This altitude

correction has been used to produce an updated ERBS Nonscanner WFOV Edition3 dataset.

The ERBS Nonscanner WFOV SW sensor dome transmission corrections determined by bi-weekly solar constant observations appear to have underestimated the change by about 1% over the first 15 years of the mission. This additional 1% correction to the SW sensor is not currently incorporated into the archived WFOV Edition3 dataset and can result in an additional 1 Wm^{-2} correction to the decadal changes in both LW and SW fluxes. The drift correction, however, is available to data users through the WFOV Edition3 data quality summary so they can apply the correction to the WFOV Edition3 data and convert them into WFOV Edition3_Rev1 data. Overall, the combined effects of altitude correction and SW sensor drift correction change the values of the reported decadal changes in tropical mean (20N to 20S) Earth radiation budget in TOA LW/SW/net radiation between the late 1980s and the 1990s from 3.1/-2.4/-0.7 Wm^{-2} to 0.7/-2.1/1.4 Wm^{-2}, respectively.

Comparison of decadal changes in ERB with existing satellite-based decadal radiation datasets shows very good agreement among ERBS Nonscanner WFOV Edition3_Rev1, HIRS Pathfinder OLR, and ISCCP FD datasets. The AVHRR Pathfinder ERB dataset, however, does not compare well against the ERBS Nonscanner WFOV and the two other ERB datasets, either in the normal AVHRR Pathfinder data, or in the corrected AVHRR Pathfinder data. Discontinuities in the AVHRR data remain too large for detection of the climate changes shown in the other data sets.

Comparison of interannual variability of net flux anomalies between ocean heat storage data and the broadband ERB datasets shows remarkable agreement in both phase

and magnitude of these two very different types of datasets. The ocean heat storage data agree with the level of interannual variability found in the radiation data. This variation is larger than known variations in aerosol or other radiative forcings in the late 1990s, and suggests a closely linked variation in global ocean heat storage and global cloud net radiative forcing. Because phase lag is not expected between these two variables, it remains unclear if slight changes in ocean surface temperature and surface heat fluxes are changing clouds, or if clouds are changing ocean heat storage. The magnitude of the global ocean heat storage and net radiation changes have several implications for understanding climate change.

1. The new results do not support the recent Iris hypothesis (Lindzen et al. 2001**,** Lin et al. 2004). As tropical and global SST warms in the late 1990s during the 97/98 El Nino, the Iris negative feedback predicts net flux to decrease (ocean cooling) as opposed to the increase (ocean heating) seen in Figure 7.
2. The ocean heat storage and net radiation data, while showing relatively large interannual variability, are consistent with heating predicted from current state of the art coupled ocean/atmosphere climate models (Barnett, et al., 2001). The anticipated change in anthropogenic radiative forcing over the next few decades is estimated as ~ 0.6 Wm^{-2} per decade (IPCC, 2001). The interannual variability in net radiation is of similar magnitude (+/- 0.7 Wm^{-2}). Note that the ocean heat storage dataset for single annual mean values has a sampling uncertainty of 0.4 Wm^{-2} (1σ) so that the larger range of variation in ocean heat storage is more likely due to its larger sampling noise. The radiation data set has a larger mean bias uncertainty (absolute calibration) but smaller sampling error than the ocean heat storage data. The 10-year average of

ocean heat storage is about 0.6 Wm^{-2}, similar to the levels predicted by current climate models for anthropogenic global warming scenarios (IPCC 2001, Hansen et al. 2005).

3. The net radiation and ocean heat storage variability predict that studies of cloud feedback in the climate system will require extremely accurate long time series of both ocean heat storage data as well as clear-sky, all-sky and cloud radiative forcing observations. With anticipated anthropogenic radiative forcing changes of 0.6 Wm^{-2} per decade, cloud radiative forcing changes of only 0.3 Wm^{-2} per decade can represent 50% changes in climate sensitivity. Both ocean heat storage and radiation data sets will require intense examination to verify these subtle but critical changes. The GEWEX Radiation Panel is currently beginning a Radiative Flux Assessment of both TOA and surface radiative fluxes consistent with this need. Independent data sets and high accuracy and stability will be critical. Our results support the need for a 21st climate observing principle: independent observations, with independent analysis of each climate data set.
4. The data suggest that a key test of coupled climate models will be the observed interannual variations in ocean heat storage and net cloud radiative forcing. It will be necessary to unscramble these two very different physical processes in a cause and effect linkage on decadal time scales. On the basis of purely time scale, one hypothesis would suggest that the long time scale ocean dynamics variability drives the very short time scale cloud processes. But the ocean heat storage is dominated not by surface temperature change, but by changes down to depths of 1000m (Levitus, 2001; Willis et al., 2004). Near surface SST changes are not constrained on the

decadal time scale to simply follow changes in ocean heat storage. Therefore, the physical link of ocean heat storage to drive cloudiness changes is not clear. The alternative hypothesis is that changes in cloudiness are driving changes in ocean heat storage. In this scenario the cloudiness changes are the result of either systematic anthropogenic climate change (e.g. changing equator to pole temperature gradient) and/or natural variability. The ocean heating is then a response to changes in net cloud radiative forcing that modifies the surface ocean energy balance. The fully coupled system is much more complicated than described, and the examples are only meant to highlight the type of challenges ahead.

5. The ERBS Nonscanner WFOV data for November 1999 through current should be reprocessed to account for the 15-degree shift from the normal nadir pointing of these instruments on the ERBS spacecraft. The data will provide a key independent time series in the CERES time frame, and will cover the current gap in the ERB record from October 1999 (end of current ERBS processing) through February 2000 (beginning of CERES Terra data).
6. The intercomparison of the corrected ERBS Nonscanner WFOV with other radiation data sets reaffirms the critical need for overlapped and continuous climate data records. Figure 8 shows the new version of Fig.1 from Wielicki et al. (2002a) with the new ERBS WFOV Edition3_Rev1 data. The Scanner and Nonscanner records no longer agree as well as before. The disagreement, however, is within the absolute accuracy of the instruments for calibration of SW and LW fluxes: 2 Wm^{-2} for ERBE and ScaRaB and 1 Wm^{-2} for CERES. As a result, for non-overlapped climate records, differences of up to 3 Wm^{-2} are within the absolute calibration uncertainty. This is

analogous to the same issue in solar constant measurements and most climate measurements. Even the most accurately calibrated instruments are typically not sufficient to handle gaps in the data record.

7. Finally, the results showed in this paper further demonstrate the need for improving the quality of the current and future ERB climate data record through a) advancing instrument absolute calibration and instrument stability performance with new technologies, b) reducing possible gaps in the climate data record with overlapped missions through advanced planning, and c) adding independent ERB observations with independent analysis to confirm climate change surprises. These are not easy tasks, but they are needed to fully understand our changing climate system.

Acknowledgments: The authors would like to thank Dr. Joel Susskind (NASA GSFC) for providing the HIRS Pathfinder OLR dataset, Dr. Lin Chambers (NASA LaRC) for editorial support, three anonymous reviewers for their constructive and valuable comments. The ERBE/ERBS Nonscanner WFOV S10N and the CERES/Terra Scanner ES4 data are provided by the NASA Langley Atmospheric Sciences Data Center in Hampton, Virginia. These data are also available directly on-line from their web site at eosweb.larc.nasa.gov. The ISCCP FD data set is obtained directly on-line from the ISCCP web site at isccp.giss.nasa.gov. The AVHRR Pathfinder ERB data set is obtained on-line from the NOAA web site at www.saa.noaa.gov. The NASA Science Mission Directorate through the CERES project at Langley Research Center funded this study.

APPENDIX A

ERBE Nonscanner Science Algorithm and Data Processing

The ERBE/ERBS Nonscanner WFOV S10N dataset has gone through two major reprocessings and one user-applied adjustment since the original data began public release in the late 1980's. The original version of the ERBE/ERBS Nonscanner data spans the 11-year period between November 1984 and October 1995. The Edition 2 dataset were released in 2002 to reduce monthly mean diurnal cycle noise in single satellite data products by removing data that contains large temporal sampling errors in a given month. The errors are driven by incomplete sampling during the 72-day orbit precession through 24 hours of local time. Errors are largest at high latitudes. Edition 2 data covers the 15-year period from November 1984 to September 1999.

Both the Edition 3 and the user-applied Edition3_Rev1 dataset, which are the subject of this paper, were released in 2005 to correct for subtle changes in TOA fluxes due to (1) a small decrease over time in the ERBS satellite altitude and (2) a small Nonscanner SW sensor drift, respectively, over the same 15-year period. While the ERBS Nonscanner WFOV S10N dataset have gone through these three major editions over the years, the basic science algorithm and data processing system that were used to process these data have remained unchanged. This basic processing system contains three main components: calibration, inversion to instantaneous TOA flux, and time-space averaging. First, the ERBE Nonscanner hemispheric flux measurements at satellite altitude are calibrated against both the on-board blackbodies and the Sun to determine gains and offsets of the instrument (Luther et al., 1986a; Luther et al., 1986b; Lee et al., 1987). Second, the calibrated satellite altitude flux data are converted to instantaneous TOA flux

measurements using the ERBE Nonscanner inversion algorithm (Green and Smith, 1991). Third, the instantaneous TOA flux data are temporally averaged to produce monthly mean datasets using the ERBE time-space averaging algorithm (Brooks and Minnis, 1984).

Edition2 data adds an additional monthly data quality control algorithm (Smith et al., 2000) to the basic data processing system. Edition3 and Edition3_Rev1 data incorporate algorithms (current paper) for further correcting the subtle but significant effects of satellite altitude change and shortwave instrument drift due to non-uniform exposure to UV radiation, respectively, to this 15-year dataset. An additional change in more recent analysis using the daily ERBS data is the use of 36-day means for tropical data (20S to 20N) and 72-day means for all latitudes (Wielicki et al., 2002b). These are the 12-hour and 24-hour local solar time precession periods of the ERBS spacecraft orbit. The 36-day averaging period is sufficient in the tropics to cover the full 24 hours of local time sampling because of the 12 hour local time difference of day and night ERBS orbit crossings near the equator. At latitudes of 40 to 60 degrees, however, the full 72-day precession cycle is required to cover all 24 hours of local time with the ERBS 57 degree inclination orbit. This is true of any precessing satellite orbit near the latitude of the satellite inclination.

APPENDIX B

Uncertainty of Long-Term TOA Radiation Datasets

Determining the uncertainty associated with TOA radiative flux climate data sets is complicated by the large number of different error sources in such complex scientific datasets. This is the reason that the GEWEX Radiation Panel is currently conducting a Radiative Flux Assessment of both TOA and surface radiative fluxes to address this particular issue and to understand the consistency among various flux datasets. Uncertainty in any TOA radiative flux dataset results from a combination of factors including calibration, spectral sampling, angular sampling, spatial sampling, temporal sampling, as well as algorithm changes. A discussion of these error sources as well as a detailed table of estimated errors for the ERBE and CERES scanner TOA fluxes can be found in Wielicki et al. (1995). Direct comparisons of ERBE scanner and nonscanner active cavity data can be found in Green et al. (1990).

The uncertainty estimates are developed using a combination of laboratory and in-orbit calibration data, internal consistency checks, theoretical error analyses, sensitivity studies, and observational studies of related independent data sources. The results are then combined together to give a total uncertainty statement of the dataset. Although this is the best uncertainty estimate at time of the data release, the dataset itself may still contain systematic biases due to undiscovered instrument changes, algorithm errors, or code errors. These systematic biases can only be corrected during major data processing efforts once the sources of the physical errors are identified and methods for removing them are determined and validated.

Absolute accuracy and stability are two critical physical quantities that define the radiometric performance of scientific instruments for climate records. It is important to point out that the long-term stability of a climate instrument and its sampling of the earth system plays a much greater role in long-term climate change studies than the precision or short-term noise in the same dataset. For example, a climate dataset with excellent precision but poor stability with time has little science value for decadal climate change studies. On the other hand, a stable climate data record with relative large short time scale errors can be extremely useful for climate change study. Climate change detection, therefore, requires climate datasets with great stability, including stable instrumentation, stable input data sources, stable sampling of space and time including diurnal cycles, and stable science algorithms and data processing systems. Instrument stability can only be achieved by using a combination of careful pre-launch instrument design and characterization as well as post-launch monitoring using accurate on-broad calibration systems and data consistency checks with other available data sources. A more complete discussion can be found in the report of an interagency workshop on satellite calibration requirements in Ohring et al. (2005). As noted in that report, the ideal situation is absolute accuracy sufficient to directly measure decadal changes from different instruments. However, this is often difficult to achieve and further advances in instrument technology are needed to overcome this limitation. The second best, and more practical, approach is sufficient stability within each instrument to measure decadal change, but with absolute errors no larger than a factor of 5 to 10 worse than the stability requirement. The logic is that larger absolute accuracy error will allow aliasing of

secondary effects to appear as spurious climate signals, even if the measurement itself is stable.

The ERBS Nonscanner WFOV dataset is the only stable long-term climate dataset that is based on broadband flux measurements. The ERBS WFOV instrument is an active cavity radiometer designed to measure broadband hemispheric fluxes. The major sources of uncertainty for this dataset include those of calibration, angle sampling, spatial sampling, and temporal sampling. The total uncertainty for the WFOV longwave and shortwave is estimated by Green et al. (1990) to be on the order of 2.5 Wm^{-2} or 2.5% of SW TOA reflected flux, and 1% of LW TOA emitted flux. For decadal changes and interannual variations as shown in the current paper, however, the more relevant error analysis is for annual mean changes in the tropics and 60S to 60N over the 1985 to 1999 time period. Below we consider the four major error sources (calibration, angle sampling, time sampling, space sampling) and briefly summarize results documenting these uncertainty levels.

The ERBS Nonscanner WFOV calibration stability uncertainty is an order magnitude better than its total uncertainty and is estimated from observations to be on the order of 0.35 Wm^{-2} over the 1985 to 1999 time period of the Edition 3 Revision 1 ERBS data. Specifically, the total channel ERBS Nonscanner WFOV active cavity radiometer, which controls the ERBS net radiation estimation, has shown stability in solar calibrations of 0.1% or 0.35 Wm^{-2} in Earth reflected SW plus emitted LW flux over the 15-year period from November 1984 to September 1999, when compared to other solar constant satellite missions by Lee et al. (2003). This is equivalent to a stability of 0.2 Wm^{-2} per decade for Net flux. Note that Net flux trends are controlled by the ERBS Total channel alone, and

not by the SW channel. Any calibration changes in the SW channel only affect the relative changes of SW and LW fluxes. The WFOV SW calibration is also determined from solar constant comparisons, and is corrected in the current paper to account for non-uniform transmission loss over the SW filter dome. The filter dome correction from Figure 3 of this paper has a total change of ~1% per decade in SW flux, and a 95% confidence uncertainty on the slope of 0.1% per decade.

Annual mean spatial sampling errors for the tropical (20S to 20N) and 60S to 60N regions are less than 0.1 Wm^{-2}. The estimate is obtained by scaling the results of Green and Smith (1991) for spatial and angular sampling errors with the WFOV ERBS sensor. While the WFOV sees limb to limb on the Earth from the 600 km ERBS orbit altitude, Green and Smith (1991) showed that the equivalent diameter of the WFOV instantaneous observations are ~1500km. Given ERBS 2700km typical orbit track separation at the equator, ERBS requires roughly 2 days to view the entire earth from 60S to 60N.

Since the WFOV sees the entire hemisphere of radiation, it is relatively insensitive to angular sampling errors. Angle sampling sensitivity tests by Green et al. (1990) show that 30% changes in earth's radiation anisotropy from nadir to limb are required to cause global annual WFOV TOA flux changes of 2 Wm^{-2} for SW flux and 1 Wm^{-2} for LW flux. Angle sampling patterns for the ERBS orbit have not varied over the mission lifetime, unlike drifting NOAA sun-synchronous orbits with changing local times of observation and solar zenith angle from year to year. Even 3% changes in earth's global average anisotropy would be very large for decadal change, so that uncertainty in decadal change for ERBS WFOV due to angle sampling are estimated at less than 0.2 Wm^{-2} for SW flux and 0.1 Wm^{-2} for LW flux.

For time sampling errors, the ERBS spacecraft orbit samples the entire 24 hour diurnal cycle every 72 days, or close to 5 times per year. Sampling studies were carried out using 3-hourly geostationary data subsampled over the tropics at the ERBS orbit times to determine diurnal sampling errors for monthly means. Wielicki et al. (2002a,b) showed that the 20S to 20N monthly mean ERBS WFOV SW flux error is 1.7 Wm^{-2} and LW flux diurnal sampling error is 0.4 Wm^{-2}. They also showed that use of orbit precession cycle means of 36 days for the tropics (72 days for 60S to 60N) dramatically reduce time sampling errors. If the errors were random, annual mean errors would be reduced by a factor of 3.5 (or square root 12 months). This suggests annual tropical mean uncertainties of 0.5 Wm^{-2} for SW and 0.1 Wm^{-2} for LW flux. In fact, because of the systematic aliasing of ERBS diurnal sampling between 30-day months and the 72-day orbit precession cycle discussed in Wielicki et al. (2002b), the errors are reduced even further than random noise when averaged over an entire year of 5 precession cycles for the annual mean. A full error simulation of this effect has not been carried out, but the 0.5 and 0.1 Wm^{-2} time sampling error estimate for annual mean should be considered an upper bound on time sampling error. More realistic values are likely a factor of 1.5 to 2 smaller. A factor of 1.5 is assumed here.

When the four ERBS error sources are combined, the total stability uncertainty (1-sigma) in the 60N to 60S and tropical annual mean radiation for the ERBS WFOV 15-year dataset from all three sources combined is on the order of 0.3 to 0.4 Wm^{-2}. Time sampling uncertainty dominates SW and Net flux stability, while calibration uncertainty dominates LW flux stability.

The other long-term TOA datasets in this paper are simulated broadband flux data products based on narrowband radiance measurements. The HIRS Pathfinder OLR and the ISCCP FD dataset are conceptually similar products. Both products use a radiative transfer model to simulate broadband TOA fluxes using inputs of cloud properties, atmospheric profile, and surface conditions derived from narrowband radiances. The AVHRR Pathfinder data, on the other hand, uses a different approach and simulates the broadband TOA flux from narrowband radiance measurements using a narrow to broadband regression technique. While these simulated broadband flux datasets were validated against broadband measurements from ERBE and/or CERES, there is not sufficient information in the existing literature to determine the long-term stability of these data products. For example, Mahta and Susskind (1999) gave an uncertainty of 5 Wm^{-2} for the HIRS Pathfinder OLR dataset when compared with 5-year of ERBE scanner data. Zhang et al. (2004) put the uncertainty of the ISCCP FD data set at 10-15 Wm^{-2} in the shortwave and 5-10 Wm^{-2} in the longwave radiation when compared with ERBE and CERES data. The uncertainty of the AVHRR Pathfinder ERB data is estimated to be on the order of 10 Wm^{-2} in shortwave and 5 Wm^{-2} in longwave radiation when compared with ERBE scanner data (Stowe et al., 2002). These uncertainty estimates, however, are not very useful for assessing the stability of these climate datasets since they are more closely related to the data precision uncertainty (i.e., mean differences between ERBE and the simulated broadband dataset for some short period of time). The long-term stability uncertainty of these simulated broadband dataset can only be obtained through direct comparison with long-term true broadband dataset from the same data period. Based on results from the current study, we conclude that the long-term

stability uncertainty of the HIRS Pathfinder OLR and the ISCCP FD dataset are very similar to those of the ERBS Nonscanner WFOV Edition3_Rev1 dataset. The long-term stability uncertainty of the AVHRR Pathfinder ERB data, on the hand, is currently too large to be useful for climate change study.

REFERENCES

Barkstrom, B. R., 1984: The Earth Radiation Budget Experiment (ERBE). *Bull. Amer. Meteor. Soc*., **65**, 1170-1185.

Barnett, T. P., D. W. Pierce, and R. Schnur, 2001: Detection of anthropogenic climate change in the world's ocean. *Science*, **292**, 270-274.

Bess, T. D., G. L. Smith, and T. P. Charlock, 1989: A Ten-year Monthly Data Set of Outgoing Longwave Radiation from Nimbus-6 and Nimbus-7 Satellite. *Bull. Amer. Meteor. Soc*., **70**, 480-489.

Brooks, D. R. and P. Minnis, 1984: Simulation of the Earth's monthly average regional radiation balance derived from satellite measurement. *J. Climat & Appl. Meteorol*, **23**, 392-403.

Duvel, J.-Ph., M. Viollier, P. Raberanto, R. Kandel, M. Haeffelin, L. A. Pakhomov, V. A. Golovko, J. Mueller, R. Stuhlmann, and the International ScaRaB Scientific Working Group, 2001: The ScaRaB-Resurs Earth Radiation Budget Dataset and First Results. *Bull. Amer. Metero. Soc*., **82**, 1397-1408.

Gordon, C. T., A. Rosati, and R. Gudgel, 2000: Tropical Sensitivity of a Coupled Model to Specified ISCCP Low Clouds. *J. Climate*, **13**, 2239-2260.

Green, R. N., F. B. House, P. W. Stackhouse, X. Wu, S. A. Ackerman, W. L. Smith, and M. J. Johnson, 1990: Intercomparison of Scanner and Nonscanner Measurements for the Earth Radiation Budget Experiment. *J. Geophys. Res.,* **95,** 11,785-11,798.

Green, R. N. and G. L. Smith, 1991: Shortwave Shape Factor Inversion of Earth Radiation Budget Observation. *J. Atmos. Sci*., **48**, 390-402.

Hansen, J., L. Nazarenko, R. Ruedy, M. Sato, J. Willis, A. Del Genio, D. Koch, A. Lacis,

K. Lo, S. Menon, T. Novakov, J. Perlwitz, G. Russell, G. A. Schmidt, and N. Tausnev, 2005: Earth's Energy Imbalance: Confirmation and Implications. *Science*, **308**, 1431-1435.

IPCC, 2001: Climate Change 2001: The Scientific Basis. Cambridge University Press, 870 pp.

Jacobowitz, H., L. L. Stowe, G. Ohring, A. Heidinger, K. Knapp, and N. R. Nalli, 2003: The Advanced Very High Resolution Radiometer Pathfinder Atmosphere (PATMOS) Climate Dataset: A Resource for Climate Research. *Bull. Amer. Meteor. Soc*., **84**, 785-793.

Kandel, R., M. Viollier, P. Raberanto, J.-Ph. Duvel, L. A. Pakhomov, V. A. Golovko, A. P. Trishchemko, J. Muller, E. Raschke, R. Stuhlmann, and the International ScaRaB Scientific Working Group, 1998: The ScaRaB Earth Radiation Budget Dataset. *Bull. Amer. Meteor. Soc*., **79**, 765-783.

Kiehl, J. T., J. J. Hack, G. B. Bonan, B. A. Boville, D. L. Williamson, and P. J. Rasch, 1998: The National Center for Atmospheric Research Community Climate Model: CCM3. *J. Climate*, **11**, 1131-1149.

Kistler, R., W. Collins, S. Saha, G. White, J. Woollen, E. Kalnay, M. Chelliah, W. Ebisuzaki, M. Kanamitsu, V. Kousky, H. V. D. Dool, R. Jenne, and M. Fiorino, 2001: The NCEP-NCAR 50-Year Reanalysis: Monthly Means CD-ROM and Documentation. *Bull. Amer. Meteor. Soc*., **82**, 247-267.

Lau, N. C., and M. J. Nath, 2001: Impact of ENSO on SST Variability in the North Pacific and North Atlantic: Seasonal Dependence and Role of Extratropical Sea-Air Coupling. *J. Climate*, **14**, 2846-2866.

Lee, R. B., III, B. R. Barkstrom, and R. D. Cess, 1987: Characteristics of the Earth Radiation Budget Experiment solar monitors. *Applied Optics*, **26**, 3090-3096.

----, J. Paden, D. K. Pandey, R. S. Wilson, K. A. Bush, and G. L. Smith, 2002: On-obrit radiometric calibrations of the ERBE active-cavity radiometers on the Earth Radiation Budget Satellite (ERBS): 1984-2002. *Proceedings of SPIE*, **4814**, 7-10 July 2002, Seattle, Washington, USA, 369-379.

----, G. L. Smith, K. A. Bush, J. Paden, D. K. Pandey, R. S. Wilson, and K. J. Priestley, 2003: On-obrit calibrations of the ERBE active-cavity radiometers on the Earth Radiation Budget Satellite (ERBS): 1984-2002. *Proceedings of SPIE*, **5234**, 8-10 September 2003, Barcelona, Spain, 433-444.

Levitus, S., J. I. Antonov, J. Wang, T. L. Delworth, K. W. Dixon, and A. J. Broccoli, 2001: Anthropogenic Warming of Earth's Climate System. *Science*, **292**, 267-270.

Lin, B, T. Wong, B. A. Wielicki and Y. Hu. 2004: Examination of the Decadal Tropical Mean *ERBS* Nonscanner Radiation Data for the Iris Hypothesis. *J. Climate*, **17**, 1239–1246.

Lindzen, R. S., M.-D. Chou, and A. Y. Hou, 2001: Does the Earth Have an Adaptive Iris? *Bull. Amer. Met. Soc.*, **82**, 417-432.

Luther, M. R., J. E. Cooper, and G. R. Taylor, 1986a: The Earth Radiation Budget Experiment Nonscanner instruments. *Reviews of Geophysics*, **24**, 391-399.

----, R. B. Lee III, B. R. Barkstrom, J. E. Cooper, R. D. Cess, and C. H. Duncan, 1986b: Solar calibration results from two Earth Radiation Budget Experiment Nonscanner instruments. *Appl. Optics*, **25**, 540-545.

Mehta, A., and J. Susskind, 1999: Outgoing Longwave Radiation from the TOVS Pathfinder Path A Data Set. *J. Geophys. Res*., **104**, D10, 12,193-12,212.

Ohring, G., B. A. Wielicki, R. Spencer, B. Emery, R. Datla, 2005. Satellite Instrument Calibration for Measuring Global Climate Change: Report of a Workshop. *Bull. Amer. Met. Soc*., **86**, 1303-1313.

Pope, V. D., M. L. Gallani, P. R. Rowntree, R. A. Stratton, 2000: The impact of new physical parameterizations in the Hadley Centre climate model: HadAM3. *Climate Dynamics,* **16**, 123-146.

Sexton, D. M. H., D. P. Rowell, C. K. Folland, D. J. Karoly, 2001: Detection of anthropogenic climate change using an atmospheric GCM. *Climate Dynamics*, **17**, 669-685.

Smith, G. L., T. Wong, and K. A. Bush, 2000: Results of a Stochastic Quality Assurance Algorithm for Radiation Budget Data. *Preprints of the 15th Conference on Probability and Statistics in the Atmospheric Sciences*, 8-11 May 2002*,* Asheville, North Carolina, American Meteorological Society, 73-76.

----, R. B. Lee, and J. Paden, 2002: Dome Degradation Pattern of ERBE Wide Field-of-View Shortwave Radiometer. *Proceedings of SPIE Remote Sensing Conference*, **4881**, 23 September 2002, Agia Pelagia, Crete, Greece, 369-377.

Stowe, L. L., H. Jacobowitz, G. Ohring, K. R. Knapp, and N. R. Nalli, 2002: The Advanced Very High Resolution Radiometer (AVHRR) Pathfinder Atmosphere (PATMOS) Climate Dataset: Initial Analyses and Evaluations. *J. Climate*, **15**, 1243-1260.

Wielicki, B. A., R. D. Cess, M. D. King, D. A. Randall, and E. F. Harrison, 1995: Mission to Planet Earth: Role of Clouds and Radiation in Climate. *Bull. Amer. Met. Soc.*, **76**, 2125-2153.

----, B. R. Barkstrom, E. F. Harrison, R. B. Lee, III, G. L. Smith, and J. E. Cooper, 1996: Clouds and the Earth's Radiant Energy System (CERES): An Earth Observing System experiment. *Bull. Amer. Meteor. Soc*., **77**, 853-868.

-----, T. Wong, R. P. Allan, A. Slingo, J. T. Kiehl, B. J. Soden, C. T. Gordon, A. J. Miller, S.-K. Yang, D. Randall, F. Robertson, J. Susskind, and H. Jacobowitz, 2002a: Evidence for Large Decadal Variability in the Tropical Mean Radiative Energy Budget. *Science*, **295**, 841-844.

-----, A. D. Del Genio, T. Wong, J. Chen, B. E. Carlson, R. P. Allan, F. Robertson, H. Jacobowitz, A. Slingo, D. Randall, J. T. Kiehl, B. J. Soden, C. T. Gordon, A. J. Miller, S.-K. Yang, and J. Susskind, 2002b: Response: Changes in Tropical Clouds and Radiation. *Science*, **296**, 2095a.

Willis, J., D. Roemmich, and B. Cornuelle, 2004: Interannual Variability in Upper-Ocean Heat Content, Temperature, and Thermosteric Expansion on Global Scales. *J. Geophys. Res.,* **109**, C12036, doi:10.1029/2003JC002260, 13pp.

Zhang, Y., W. B. Rossow, A. A. Lacis, V. Oinas, and M. I. Mishchenko, 2004: Calculation of radiative fluxes from the surface to top of atmosphere based on ISCCP and other global data sets: Refinements of the radiative transfer model and the input data. *J. Geophys. Res*., **109**, D19105, doi:10.1029/2003JD004457, 27pp.

FIGURE CAPTIONS

Figure 1. Time series of ERBS altitude (km) above sea level from 1985 to 1999.

Figure 2. Time series of ERBS Nonscanner WFOV deseasonalized tropical mean (20N to 20S) broadband radiation budget anomalies (longwave, shortwave, and net) from 1985 to 1999 with (solid colored lines, Edition3 data) and without satellite altitude correction (black dotted lines, Edition2 data). Anomalies are defined with respect to the 1985 to 1989 period

Figure 3. Time series of ERBS Nonscanner WFOV Edition3 tropical mean (20N to 20S) daytime longwave flux (top, red curve), nighttime longwave flux (top, blue curve), and day-minus-night longwave flux differences (bottom, green curve) from 1985 to 1999.

Figure 4. Time series of ERBS Nonscanner MFOV tropical mean (20N to 20S) daytime longwave flux (top, red curve), nighttime longwave flux (top, blue curve), and day-minus-night longwave flux differences (bottom, green curve) from 1985 to 1999.

Figure 5. Comparison of time series of ERBS Nonscanner WFOV Edtion3_Rev1 deseasonalized tropical mean (20N to 20S) broadband radiation budget anomalies of longwave (top, red curve), shortwave (middle, blue curve), and net (bottom, green curve) radiation from 1985 to 1999 with both satellite altitude correction and shortwave sensor drift correction against the same time series from climate models (dashed black lines are the models mean and the shaded areas are the spread of the minimum and maximum values among models). The climate models are the same models as in Wielicki et al. (2002a).

Figure 6. Time series of deseasonalized tropical mean (20N to 20S) broadband radiation budget anomalies (longwave, shortwave, and net) from 1985 to 1999 from the ERBS Nonscanner WFOV Edition3_Rev1 (red), ISCCP FD (blue), HIRS Pathfinder OLR (pink), and AVHRR Pathfinder ERB (green) data records. Anomalies are defined with respect to the 1985 to 1989 period.

Figure 7. Interannual comparison of global ocean heat storage (blue) against global net flux anomalies from ERBE/ERBS Nonscanner WFOV Edition3_Rev1 (red) and CERES/Terra FM1 Scanner ES4 Edition2_Rev1 (green) for a 10-year period from 1993 to 2003.

Figure 8. Time series of deseasonalized tropical mean (20N to 20S) longwave anomaly (with respect to 1985 to 1989 climatology) between 1979 and 2001 based on the new ERBS Nonscanner WFOV Edition3_Rev1 (Red solid line), Nimbus7 Nonscanner (green dash line) ERBS Scanner (blue solid line), CERES/Terra FM1 Scanner ES4 Edition2_Rev1 (blue dash line), CERES/TRMM Scanner Edition2 (blue circle), ScaRaB/Meteor Scanner (green triangle), and ScaRaB/Resurs Scanner (green circle) dataset. Anomalies are defined with respect to the 1985 to 1989 period.

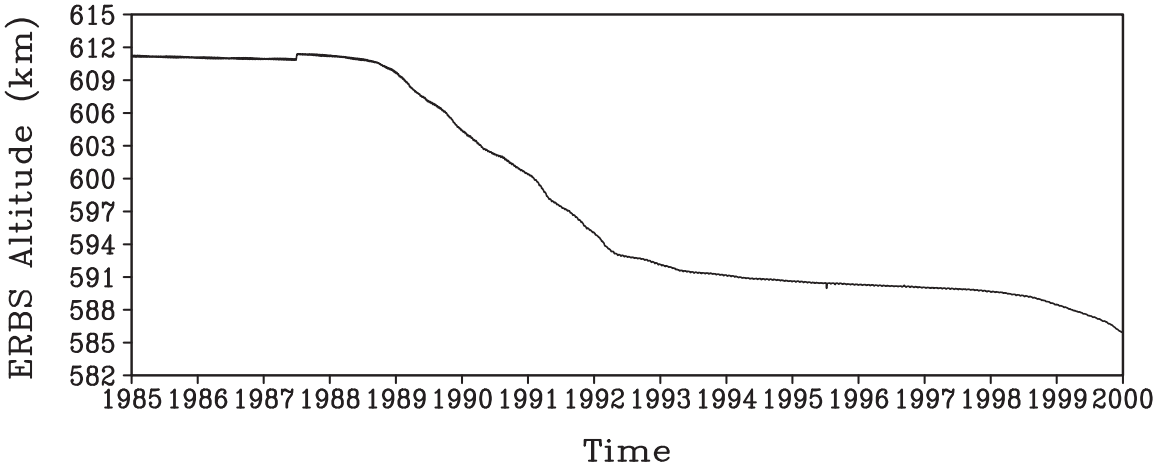

Figure 1. Time series of ERBS altitude (km) above sea level from 1985 to 1999.

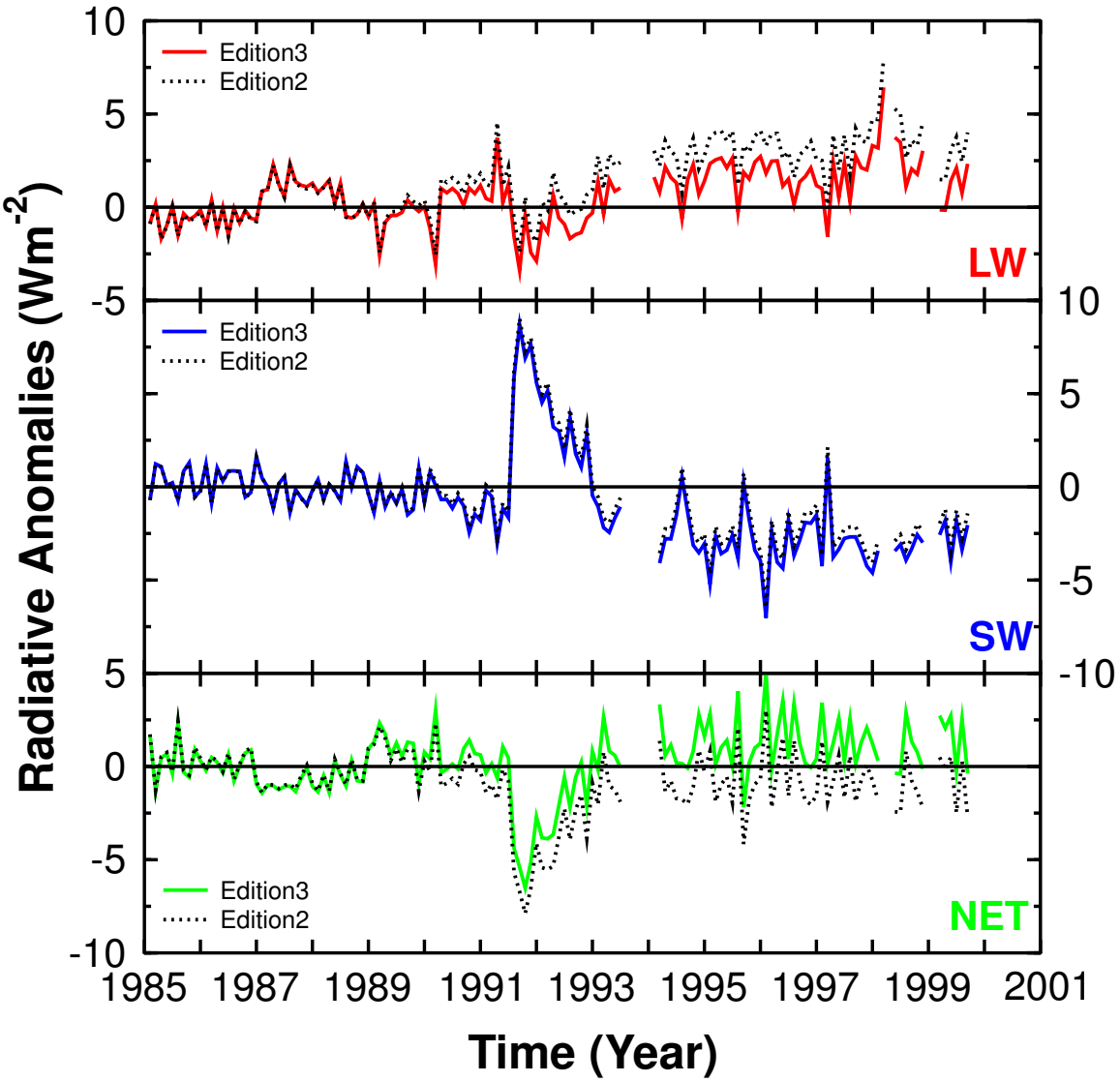

Figure 2. Time series of ERBS Nonscanner WFOV deseasonalized tropical mean (20N to 20S) broadband radiation budget anomalies (longwave, shortwave, and net) from 1985 to 1999 with (solid colored lines, Edition3 data) and without satellite altitude correction (black dotted lines, Edition2 data). Anomalies are defined with respected to the 1985 to1989 period.

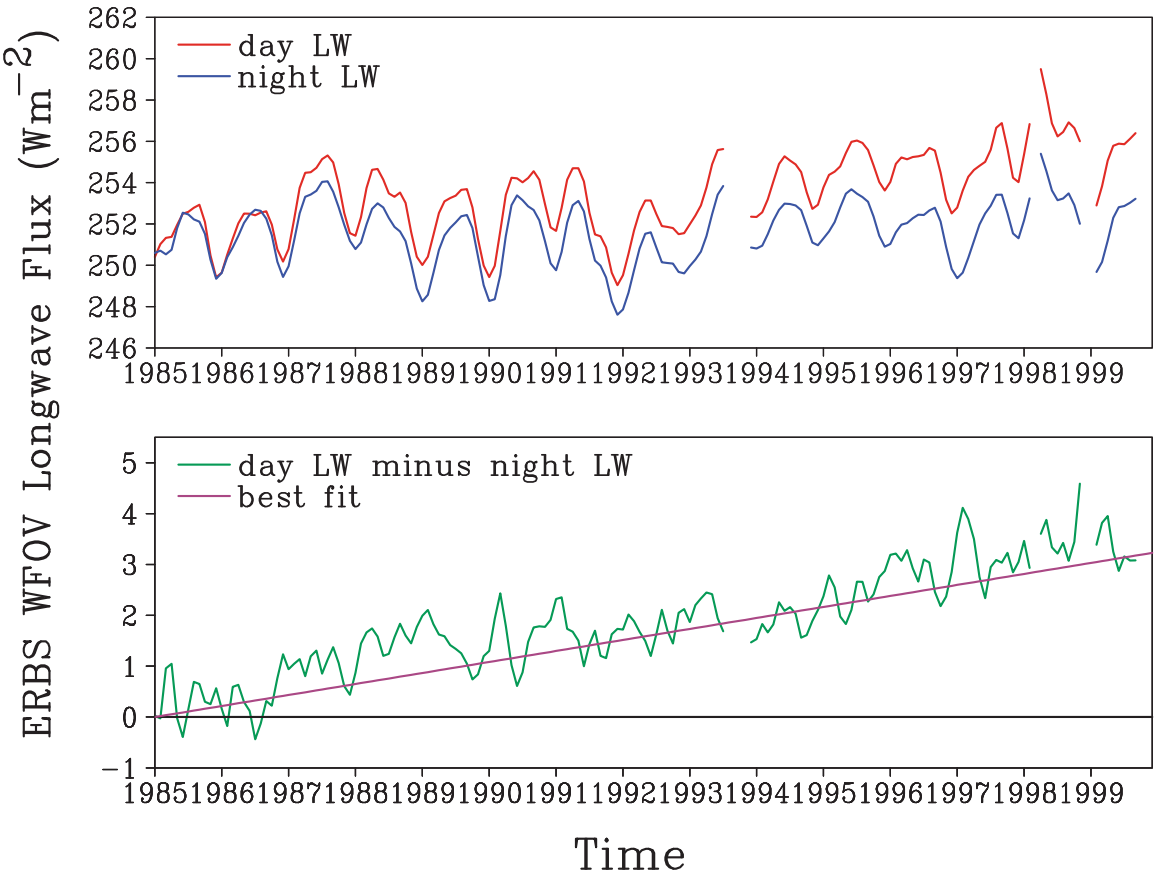

Figure 3. Time series of ERBS Nonscanner WFOV Edition3 tropical mean (20N to 20S) daytime longwave flux (top, red curve), nighttime longwave flux (top, blue curve), and day-minus-night longwave flux differences (bottom, green curve) from 1985 to 1999.

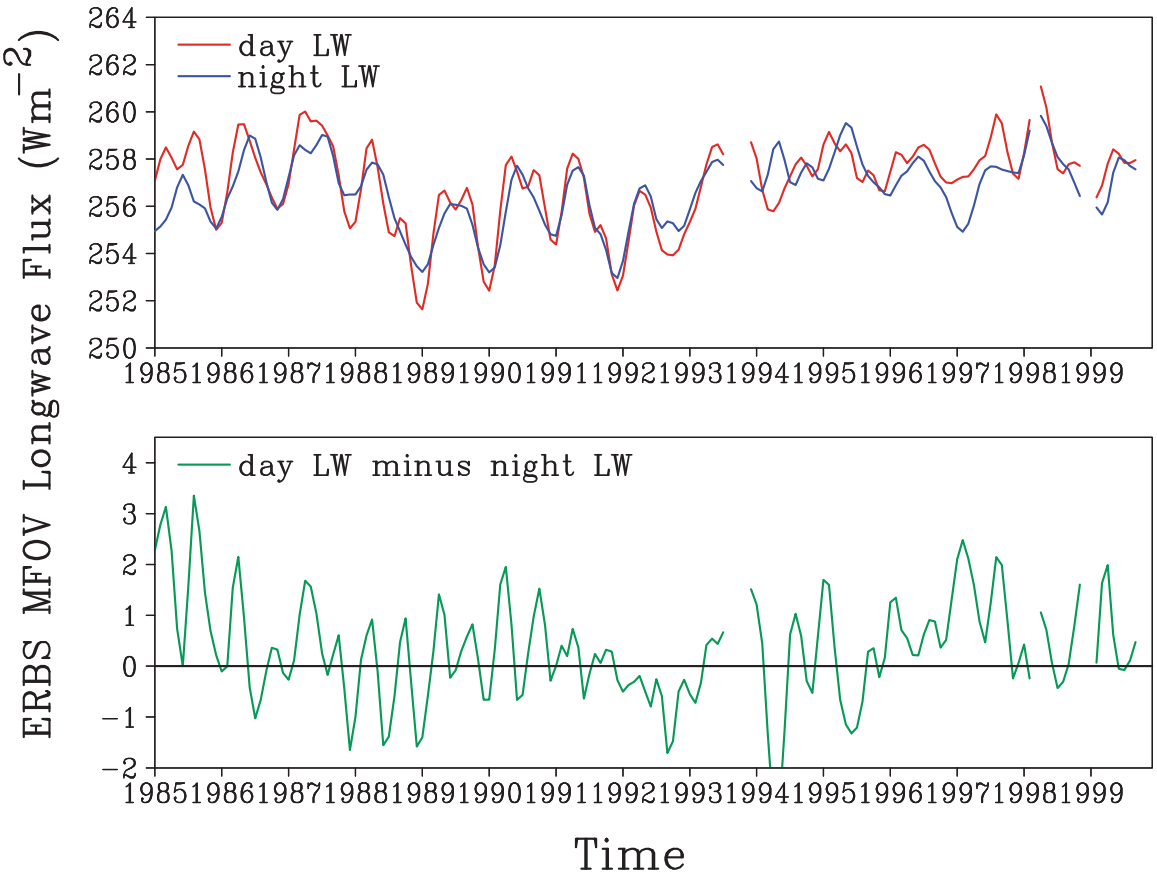

Figure 4. Time series of ERBS Nonscanner MFOV tropical mean (20N to 20S) daytime longwave flux (top, red curve), nighttime longwave flux (top, blue curve), and day-minus-night longwave flux differences (bottom, green curve) from 1985 to 1999.

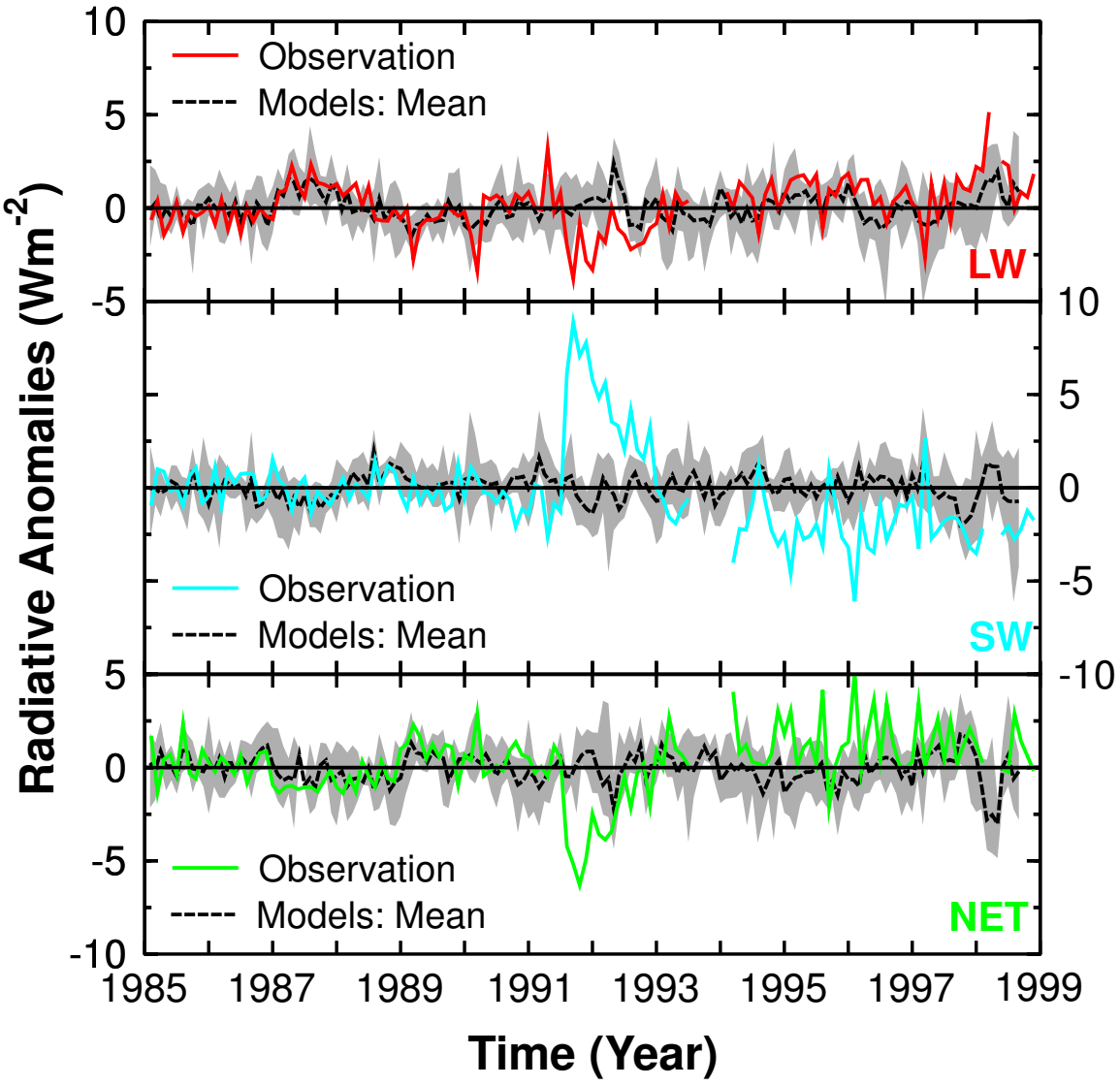

Figure 5. Comparison of time series of ERBS Nonscanner WFOV Edition3_Rev1 deseasonalized tropical mean (20N to 20S) broadband radiation budget anomalies of longwave (top, red curve), shortwave (middle, blue curve), and net (bottom, green curve) radiation from 1985 to 1999 with both satellite altitude correction and shortwave sensor drift correction against the same time series from climate models (dashed black lines are the models mean and the shaded areas are the spread of the minimum and maximum values among models). The climate models are the same models as in Wielicki et al. (2002a).

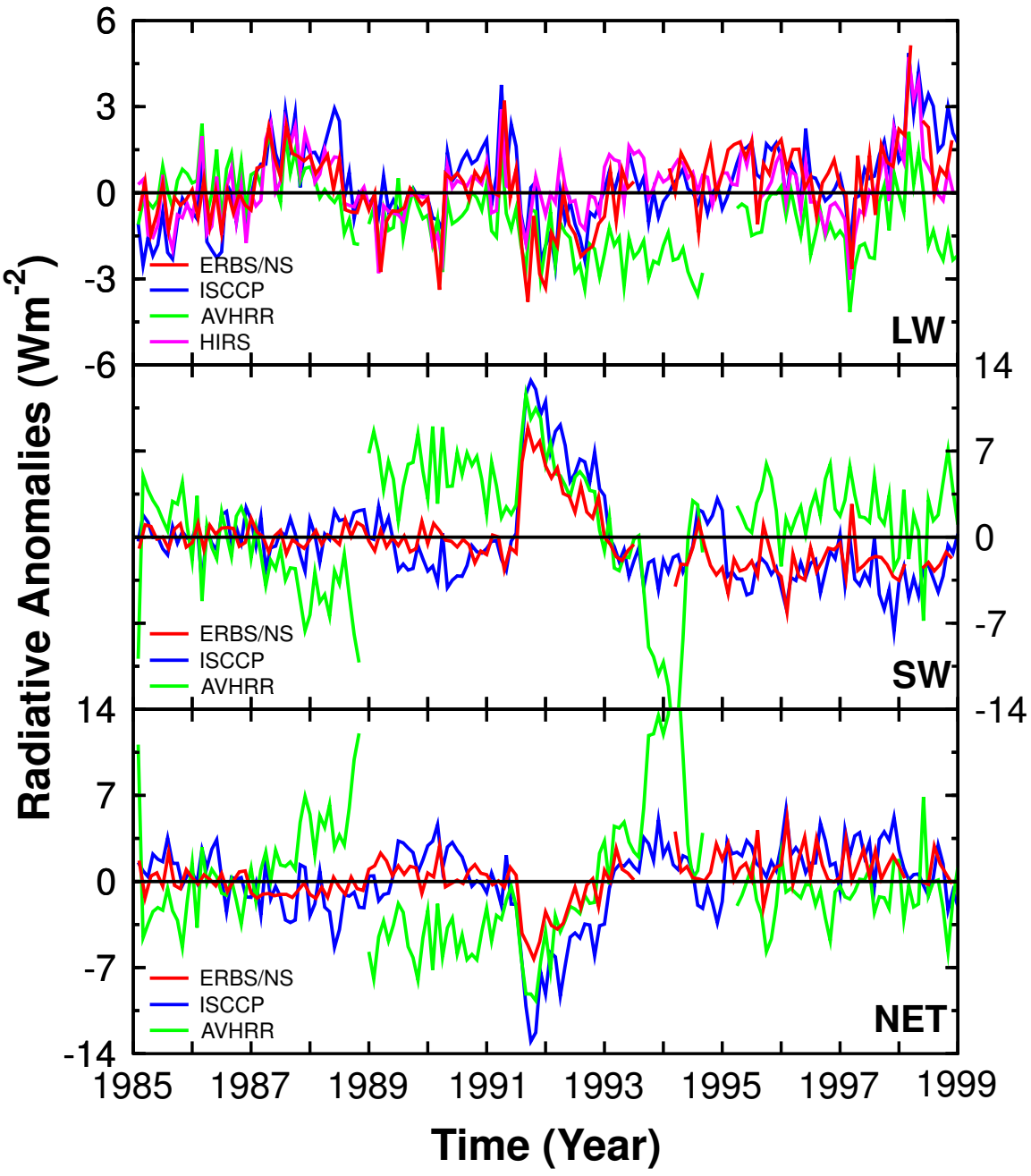

Figure 6. Time series of deseasonalized tropical mean (20N to 20S) broadband radiation budget anomalies (longwave, shortwave, and net) from 1985 to 1999 from the ERBS Nonscanner WFOV Edition3_Rev1 (red), ISCCP FD (blue), HIRS Pathfinder OLR (pink), and AVHRR Pathfinder ERB (green) data records. Anomalies are defined with respect to the 1985 to 1989 period.

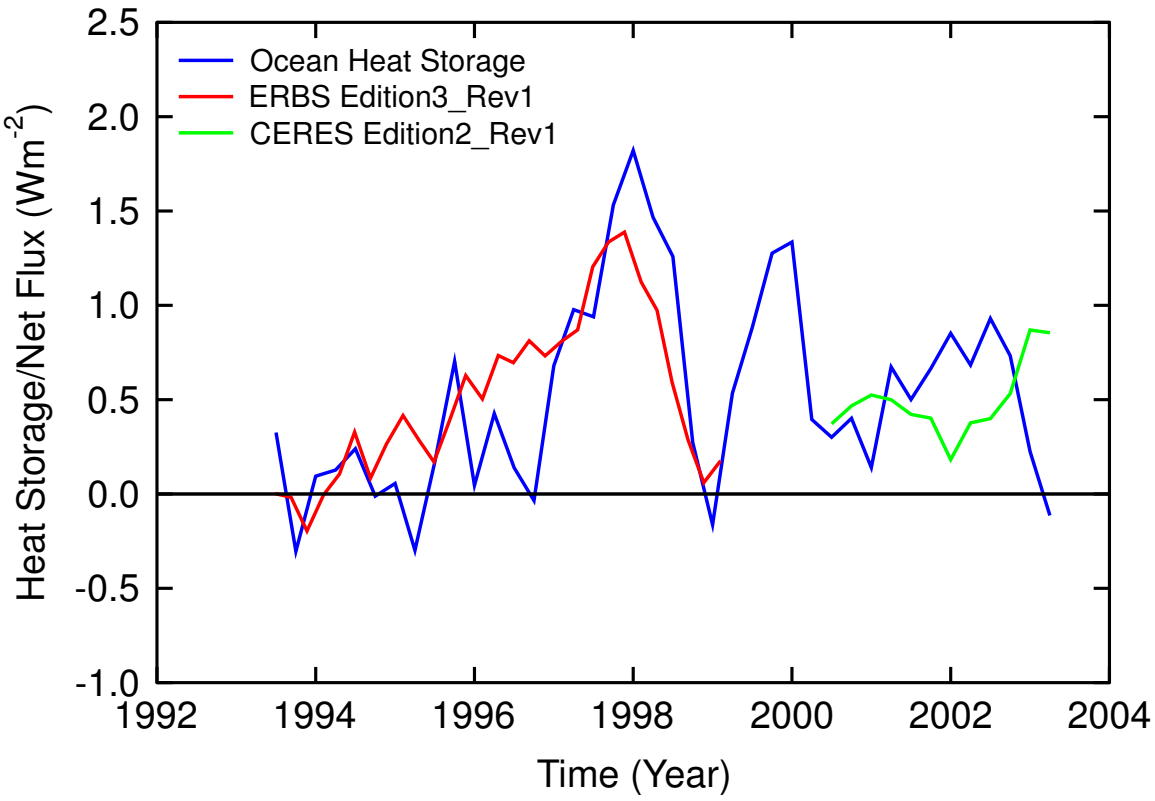

Figure 7. Interannual comparison of global ocean heat storage (blue) against global net flux anomalies from ERBE/ERBS Nonscanner WFOV Edition3_Rev1 (red) and CERES/Terra FM1 Scanner ES4 Edition2_Rev1 (green) for a 10-year period from 1993 to 2003.

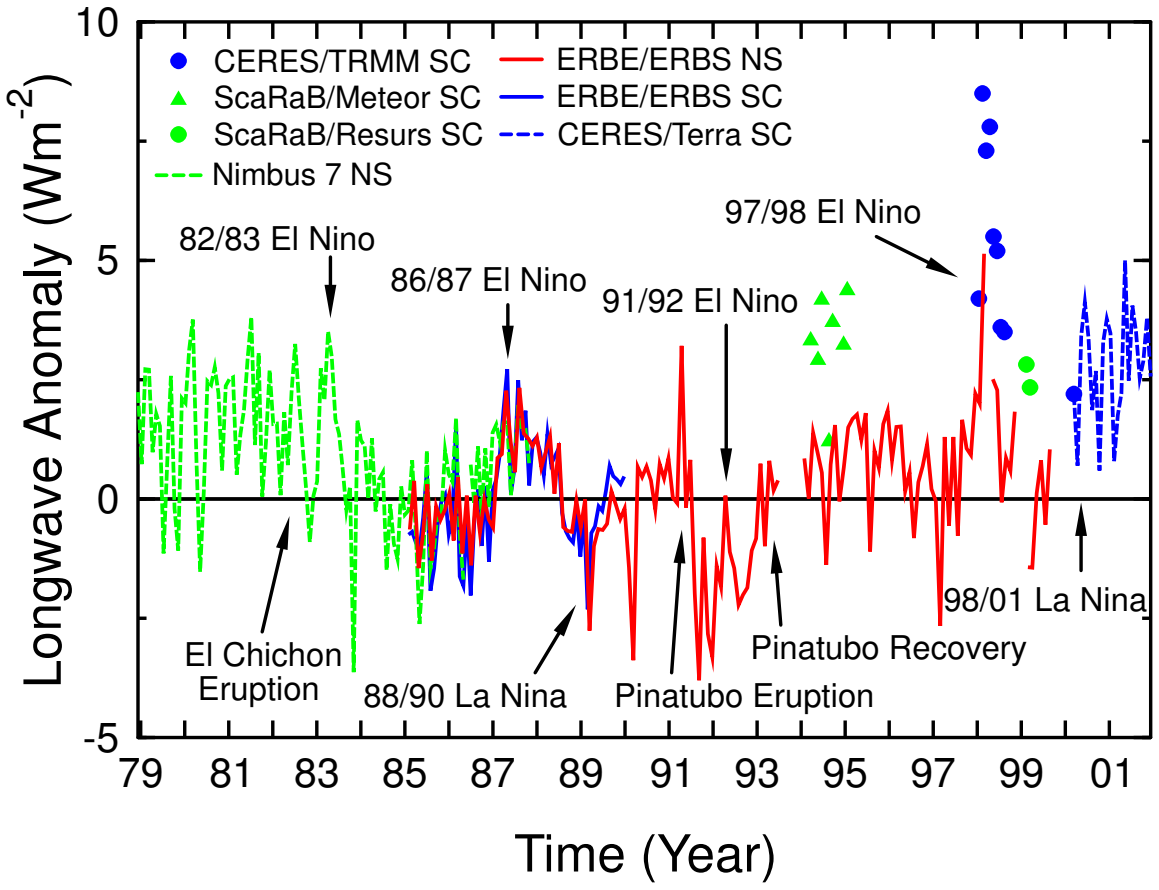

Figure 8. Time series of deseasonalized tropical mean (20N to 20S) longwave anomaly (with respect to 1985 to 1989 climatology) between 1979 and 2001 based on the new ERBS Nonscanner WFOV Edition3_Rev1 (Red solid line), Nimbus7 Nonscanner (green dash line), ERBS Scanner (blue solid line), CERES/Terra FM1 Scanner ES4 Edition2_Rev1 (blue dash line), CERES/TRMM Scanner Edition2 (blue circle), ScaRaB/Meteor Scanner (green triangle), and ScaRaB/Resurs Scanner (green circle) dataset. Anomalies are defined with respect to the 1985 to 1989 period.

TABLES

Table 1. TOA radiative flux changes (Wm^{-2}) from the 1980s to 1990s from different datasets. Values are given as tropical mean (20N to 20S) for the 1994-1997 period minus the 1985-1989 period. Dashes are shown where no data is available.

Data Source	TOA LW	TOA SW	TOA Net
ERBS WFOV Edition 2	3.1	-2.4	-0.7
ERBS WFOV Edition3	1.6	-3.0	1.4
ERBS WFOV Edition3_Rev1[1]	0.7	-2.1	1.4
HIRS Pathfinder	0.2	_	_
AVHRR Pathfinder[2]	-1.4	0.7	0.7
ISCCP FD	0.5	-2.4	1.8

[1]ERBS WFOV Edition3 with additional user-applied SW sensor drift adjustment

[2]Original uncorrected AVHRR Pathfinder data